ISSN 1674-1056
http://cpb.iphy.ac.cn
http://iopscience.iop.org/cpb
中国物理 B
Chinese Physics
中国物理
Chinese Physics B

The superconducting properties in Pb/$MoTe_2$/Pb heterostructure:First-principles calculations within the anisotropic Migdal-Eliashberg theory

Wei Xia(夏威), Jie Zhang(张洁), Gui-Qin Huang(黄桂芹)

Citation: Chin. Phys. B . 2018, 27(12): 126302. **doi:** 10.1088/1674-1056/27/12/126302
Journal homepage: http://cpb.iphy.ac.cn; http://iopscience.iop.org/cpb

What follows is a list of articles you may be interested in

A single-crystal neutron diffraction study on magnetic structure of $CsCo_2Se_2$

Juanjuan Liu(刘娟娟), Jieming Sheng(盛洁明), Wei Luo(罗伟), Jinchen Wang(汪晋辰), Wei Bao(鲍威), Jinhu Yang(杨金虎), Minghu Fang(方明虎), S A Danilkin

Chin. Phys. B . 2018, 27(11): 117401. **doi:** 10.1088/1674-1056/27/11/117401

Superconductivity with peculiar upper critical fields in quasi-one-dimensional Cr-based pnictides

Guang-Han Cao(曹光旱), Zeng-Wei Zhu(朱增伟)

Chin. Phys. B . 2018, 27(10): 107401. **doi:** 10.1088/1674-1056/27/10/107401

Superconductivity in electron-doped arsenene

Xin Kong(孔鑫), Miao Gao(高淼), Xun-Wang Yan(闫循旺), Zhong-Yi Lu(卢仲毅), Tao Xiang(向涛)

Chin. Phys. B . 2018, 27(4): 046301. **doi:** 10.1088/1674-1056/27/4/046301

Superconductivity of bilayer phosphorene under interlayer compression

Gui-Qin Huang(黄桂芹) and Zhong-Wen Xing(邢钟文)

Chin. Phys. B . 2016, 25(2): 027402. **doi:** 10.1088/1674-1056/25/2/027402

Mechanical, electronic, and thermodynamic properties of zirconium carbide from first-principles calculations

Yang Xiao-Yong, Lu Yong, Zheng Fa-Wei, Zhang Ping

Chin. Phys. B . 2015, 24(11): 116301. **doi:** 10.1088/1674-1056/24/11/116301

SPECIAL TOPIC — 60th Anniversary of the Department of Physics at the Nanjing Normal University

The superconducting properties of a Pb/$MoTe_2$/Pb heterostructure: First-principles calculations within the anisotropic Migdal–Eliashberg theory*

Wei Xia(夏威), Jie Zhang(张洁), and Gui-Qin Huang(黄桂芹)†

School of Physics and Technology, Nanjing Normal University, Nanjing 210023, *China*

(Received 29 July 2018; revised manuscript received 30 September 2018; published online 10 November 2018)

The spin-polarized band structures of an ultrathin Pb/$MoTe_2$/Pb heterostructure are calculated via first-principles density functional theory. The electron–phonon interaction and the superconducting properties of the ultrathin Pb/$MoTe_2$/Pb heterostructure are studied by using the fully anisotropic Migdal–Eliashberg theory powered by Wannier–Fourier interpolation. Due to the complex Fermi surface in this low-dimensional system, the electron–phonon interaction and the superconducting gap display significant anisotropy. The temperature dependence of the superconducting gap can be fitted by solving numerically the Bardeen–Cooper–Schrieffer (BCS) gap equation with an adjustable parameter α, suggesting that phonon-mediated mechanism as its superconducting origin. Large Rashba spin-splitting and superconductivity coexist in this heterostructure, suggesting that this hybrid low-dimensional system will have some specific applications.

Keywords: heterostructure, electron–phonon coupling, Rashba spin-splitting, superconductivity, first-principles calculation

PACS: 63.20.kd, 74.78.–w, 71.70.Ej **DOI:** 10.1088/1674-1056/27/12/126302

1. Introduction

Inspired by graphene, two-dimensional (2D) nanoscale materials are now experiencing a great surge of research interest in the field of materials science and physics because of their intriguing nanoscale structure and novel electronic and magnetic properties for applications in future nanoelectronic devices.[1–6] During the process of searching for promising materials, layered transition-metal dichalcogenides have been important members of the 2D materials. Mo and X (X = S, Se, Te) consist of stacked X–Mo–X layers, where the hexagonally packed transition metal Mo atom is typically trigonal prismatic coordinated with chalcogenide atoms X. The Mo–X bonds within one layer are covalent, but the sandwich layers are coupled only by weak van der Waals interaction,[7–9] resulting in easy cleavage of planes. Theoretical studies have revealed that indirect gap semiconductors 2H–MoX_2 become direct gap semiconductors with significantly larger gap energy than those of the bulks when thinned to a single layer.[10–16] Very recently, a long spin lifetime of more than 1 ns has been detected in polarization-resolved photoluminescence measurements,[17] demonstrating that the spin lifetimes in the MoS_2 have outpaced that in graphene. This is because the spin–orbit coupling (SOC) and absence of inversion symmetry in MoS_2 suppress spin relaxation and hence, enhances the spin lifetimes.[18] Compared to the MoS_2, $MoTe_2$ has a stronger SOC and a smaller direct energy band gap (1.1 eV)[19] in monolayer (ML), which is considered to be used for ideal valleytronic and optical devices.[20,21]

However, single material systems with restricted properties limit the development and application of the 2D materials. To date, more and more studies of TMDs are concerned with heterostructure systems.[22] One can explore an abundance of the electronic properties by stacking TMDs with metal materials.[20] In photodetection applications, the metal–TMD interface plays an active role of enhancing photoresponse.[23] The surface Co atoms tend to form highly stable ferromagnetic states and exhibit a 100% current polarization (half-metal) in the newly formed Co/MoS_2 heterostructure.[24] Rashba spin-splitting of electronic bands is found in MoS_2/Bi hybrid systems.[25]

Nanoscale metal–semiconductor structure materials occupy an important position in semiconductor and microelectronic field due to their abundant physical phenomena and effects. The ultrathin films of the heavy metal interfaced with a semiconductor substrate have received increasing attention.[26–28] By first-principles calculations, our previous work[29] has found that extremely large Rashba spin-splitting (about 350 meV) appears in the ultrathin Pb(111)/$MoTe_2$ heterostructure. The lattice mismatch at the interface of this hybrid system is very small due to the same hexagonal structure and the nearly same lattice constants of two materials. However, the electronic devices are often fabricated with two metal contacts and form a metal–semiconductor–metal structure. So here in this work, we construct ultrathin Pb(111)(1 ML)/$MoTe_2$(1 ML)/Pb(111)(1 ML) heterostructure, which has the mirror symmetry. One of the motivation

*Project supported by the Natural Science Foundation of Jiangsu Province, China (Grant No. BK20141441).

†Corresponding author. E-mail: huangguiqin@njnu.edu.cn

© 2018 Chinese Physical Society and IOP Publishing Ltd

of this work is to study the different behavior of Rashba spin-splitting from that in asymmetry Pb(111)/$MoTe_2$ heterostructure. Furthermore, many 2D materials have been found to be superconductors.[26,30–33] Pb is a conventional superconductor, so we want to know if superconductivity also appears in this ultrathin Pb(111)(1 ML)/$MoTe_2$(1 ML)/Pb(111)(1 ML) heterostructure. This is another motivation of this work. If large Rashba spin-splitting and superconductivity coexist, this heterostructure will have some novel quantum effects and specific applications. In this paper, we will systematically investigate the electronic structure and lattice dynamics of a heterostructure composed of 1-ML-$MoTe_2$ and Pb by using the first-principles method. The electron–phonon (EP) interaction and the superconducting properties are studied by using the fully anisotropic Migdal–Eliashberg theory powered by Wannier–Fourier interpolation.

2. Computational method

The optimized norm-conserving Vanderbilt pseudopotential[34] method is used with the PWSCF program of the Quantum-ESPRESSO distribution. [35] The Perdew–Burke–Ernzerhof (PBE) formulation of the generalized gradient approximation (GGA) pseudopotential, with SOC included is employed to describe the electron–electron exchange and correlation energies.[36] The highest kinetic energy in the plane-wave basis set is 80 Ry (1 Ry = 13.6056923(12) eV). Ultrathin Pb(111)/$MoTe_2$/Pb(111) is modeled by using the slab, 20-Å vacuum layers are set in order to avoid the interaction between layers. Electronic and vibrational states are computed by sampling the Brillouin zone on $(12,12,1)$ and $(6,6,1)$ grids, respectively. Maximally localized Wannier functions are determined by the WANNIER90 program.[37] For the initial projection, we use the d orbitals for the Mo atom and sp^3 hybrid orbitals for Pb and Te atoms. The electron energies, phonon frequencies and EP matrix elements on fine grids are obtained by using the Wannier–Fourier interpolation technique. The fine grids of $\boldsymbol{k}$ and $\boldsymbol{q}$ points are $(48,48,1)$ and $(24,24,1)$, respectively. The EPW program[38] is used to perform the subsequent EP interpolation and solve the anisotropic Eliashberg equations. The technical details of these calculations are described in Ref. [38].

3. Results and discussion

The stable geometric structure of 1-ML-$MoTe_2$ at ambient conditions is the 2H phase.[39] The Te atoms are arranged in a trigonal prismatic coordination of Mo atoms and the stacking of atomic planes is an $/ABA/$ sequence. For the Pb/$MoTe_2$/Pb heterostructure, because of the very small lattice mismatch, a surface (1×1) cell is used. The top and side views of the structure of Pb/$MoTe_2$/Pb heterostructure are sketched in Figs. 1(a) and 1(b). It has mirror symmetry with the Mo layer as the center plane. There are three possible sites (T_1, T_2, H_3) occupied for the contacted Pb atoms. The T_1 (T_2) site is on the Mo (Te) atom. The H_3 site is on the hollow center of the 2H hexagonal lattice. According to the calculations of the total energy after structural relaxation, the energy for H_3 site is lower than that in T_1 (T_2) site by 0.036 (0.035) eV. In the following calculations, we will only study the H_3 configuration. The stacking sequence of this configuration is $/CABAC/$, as labeled in Fig. 1(b). Our optimized lattice constant of the heterostructure is 3.524 Å, which is very close to the experimental lattice constant of $MoTe_2$ (3.52 Å).[40] The interlayer distance D between Pb and 1-ML-$MoTe_2$ is $D = 2.947$ Å, which is much smaller than interlayer distance (3.522 Å) of the bulk $MoTe_2$. After 1-ML-$MoTe_2$ is in contact with Pb, the bond length between Mo and Te (d) is increased by 1.23%. This is due to a charge transfer at the interface, which weakens the covalent bond between Mo and Te atoms.

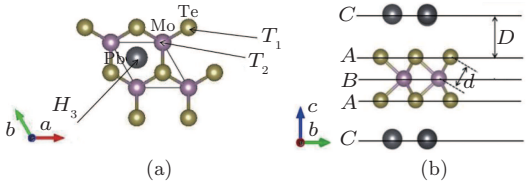


Fig. 1. (color online) Schematic crystal structures: (a) Top and (b) side views of the Pb/1ML-$MoTe_2$/Pb heterostructure.

For Pb/$MoTe_2$/Pb heterostructure, the band structure along some high symmetry directions is shown in Fig. 2(a). The corresponding Fermi surface is shown in Fig. 2(b). The green triangles in Fig. 2(a) indicate the contribution from Pb atom. The marker size is proportional to its electron density. It can be clearly seen that the bands near the Fermi energy (E_F) are mainly contributed by Pb. After spin-splitting, there are four conduction bands and four valence bands crossing the Fermi level. The Fermi surface consists of two nearly double degenerate circle-like hole pockets centered around the zone center ($\bar{\Gamma}$ point). Around the zone corner ($\bar{K}$ point), there are four arc-type electron pockets. Furthermore, the Fermi surface consists of two boat-like electron pockets at a point between $\bar{\Gamma}$ and $\bar{K}$. The band projection shows a strong hybridization between the p_z orbital of Pb and d_{z^2} of Mo for the hole bands near $\bar{\Gamma}$ point. The electron bands near the $\bar{K}$ point are mainly derived from in-plane orbitals.

The spin-splitting, *i.e.*, the Rashba effect, originates from the strong SOC and space inversion asymmetry. The Pb/$MoTe_2$/Pb heterostructure has no space inversion symmetry, but it has center mirror symmetry. The out-of-plane potential gradient equals zero, so in-plane spin polarization disappears, and it only has out-of-plane spin-polarization. This is different from the case in the asymmetric Pb/$MoTe_2$ heterostructure. Due to the time reversal symmetry between the $\bar{K}$ and $\bar{K}'$ points (labeled in Fig. 2(b)), the out-of-plane spin-polarization orientation is reversed. The largest spin-splitting occurs in the two lowest conduction bands at the $\bar{K}$ or $\bar{K}'$ points and the corresponding spin-resolved band structures are sketched in the inset of Fig. 2(a). The values of two spin-splittings are about 364 meV and 263 meV, as sketched in Fig. 2(a).

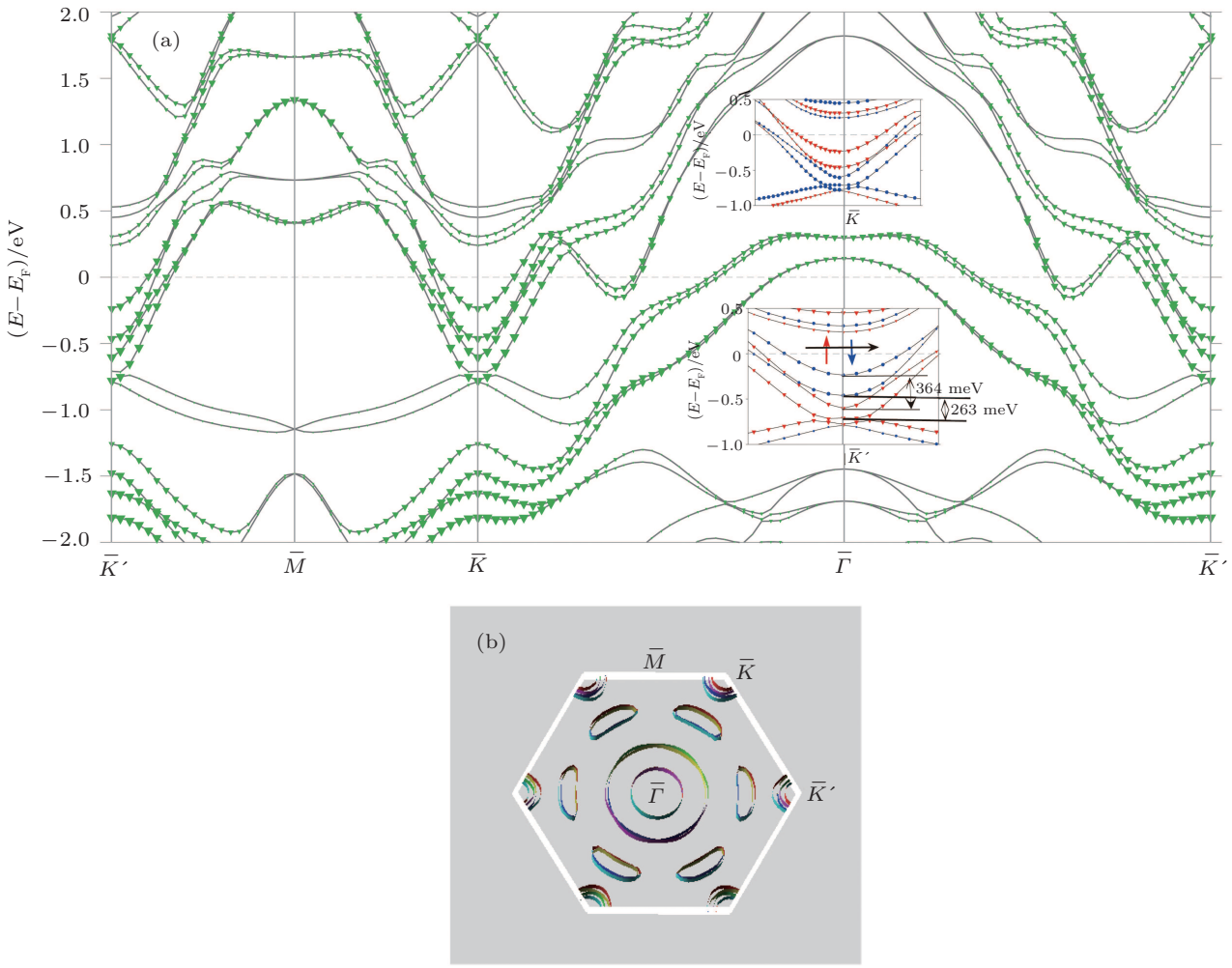


Fig. 2. (color online) (a) The band structure of the Pb/$MoTe_2$/Pb heterostructure along some high symmetry directions. Inset: out-of-plane spin-polarization bands around $\bar{K}$ and $\bar{K}'$ points; (b) the Fermi surface of the Pb/$MoTe_2$/Pb heterostructure.

The calculated phonon spectrum and the total phonon densities of states (DOS) $F(\omega)$ for the Pb/$MoTe_2$/Pb heterostructure are shown in Figs. 3(a) and 3(b). We can see that there is no imaginary frequency in the full phonon spectrum, which indicates its dynamical stability. In general, the acoustic modes and the interlayer modes between Pb and $MoTe_2$ are often in the low-frequency range, while the Mo–Te bond-stretching modes within the monolayer $MoTe_2$ are often in the high-frequency range. The calculated projected phonon DOS for the single atom is shown in Fig. 3(d). Due to the large difference of mass of the three atoms, their contribution to the phonon DOS is separated. The vibrations of Pb (Mo) atoms occupy below 6 meV (above 23 meV), while the vibrations of Te atoms occupy the middle frequency region. At the side of high-frequency, the vibrations of Mo and Te atoms are coupled.

Within the isotropic Eliashberg theory, the spectral function $\alpha^2F(\omega)$ can be given by[41,42]

$$\alpha^2F(\omega)=\frac{1}{N_F}\sum_{mn}\sum_{\nu}|g^{q\nu}_{nk,mk+q}|^2 \cdot\delta(\varepsilon_{nk}-\varepsilon_F)\delta(\varepsilon_{mk+q}-\varepsilon_F)\delta(\omega-\omega_{q\nu}). \quad (1)$$

Here, N_F is the DOS at the E_F, the $g_{mn,\nu}(k,q)$ is the EP scattering matrix element which can be determined self-consistently by the linear response theory. ε_{nk} is the energy of an electronic state $|nk\rangle$ with crystal momentum k and band index n, $\omega_{q\nu}$ is the frequency of a phonon with wave vector q and branch index ν. The frequency-dependent EP coupling reads

$$\lambda(\omega)=2\int_0^{\omega}\frac{\alpha^2F(\Omega)}{\Omega}\mathrm{d}\Omega. \quad (2)$$

Our obtained $\alpha^2F(\omega)$ and $\lambda(\omega)$ are shown in Fig. 3(c). It is found that $\alpha^2F(\omega)$ has a pronounced peak below 6 meV, which coincides well with the peak of the projected phonon DOS of Pb atoms. We obtain $\lambda(\omega=6\ \mathrm{meV})=1.14$, being about 82% of the total EP coupling $\lambda(\omega=\infty)=1.39$. So our results show that the modes from the vibrations of Pb atom have dominant contribution to the EP coupling.

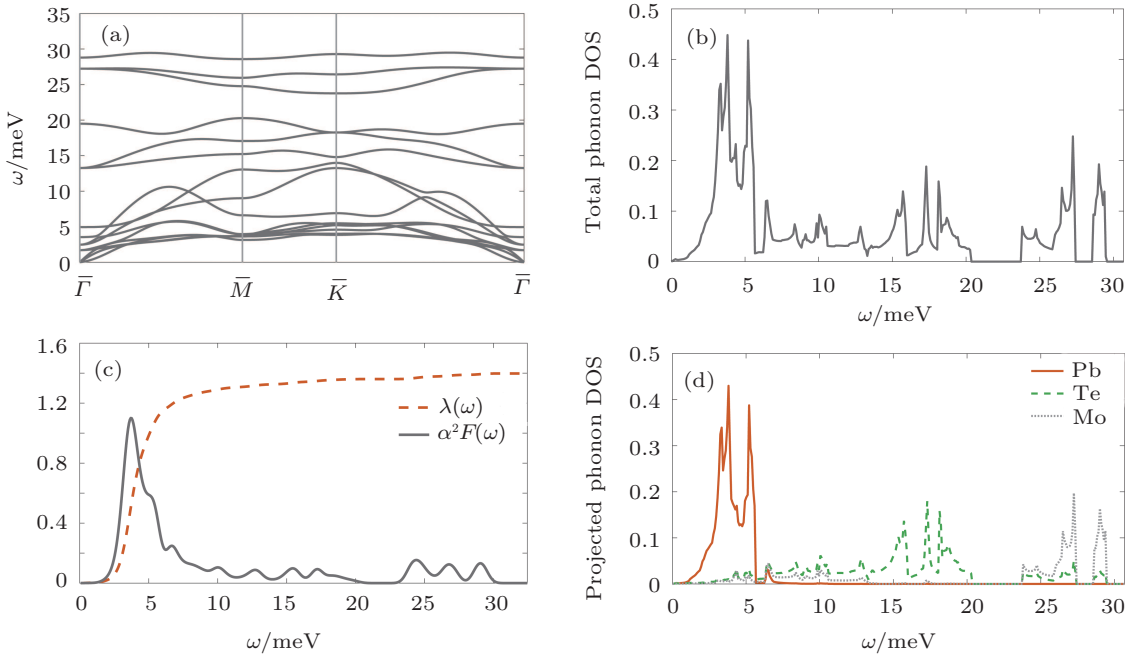


Fig. 3. (color online) (a) Phonon spectrum; (b) total phonon density of states of the Pb/$MoTe_2$/Pb heterostructure; (c) Eliashberg function $\alpha^2F(\omega)$ with integrated EP coupling constant $\lambda(\omega)$; and (d) projected phonon DOS for the Pb/$MoTe_2$/Pb heterostructure.

To study the anisotropy in the EP couping, we evaluate the crystal momentum $\boldsymbol{k}$ and the band index n-dependent EP coupling $\lambda_{n\boldsymbol{k}}$, which is given by

$$\lambda_{n\boldsymbol{k}} = \sum_{m\nu} \int_{\mathrm{BZ}} \frac{\mathrm{d}\boldsymbol{q}}{\Omega_{\mathrm{BZ}}\omega_{\boldsymbol{q}\nu}} |g_{mn,\nu}(\boldsymbol{k},\boldsymbol{q})|^2 \delta(\varepsilon_{n\boldsymbol{k}} - \varepsilon_{m\boldsymbol{k}+\boldsymbol{q}} \pm \omega_{\boldsymbol{q}\nu}), \tag{3}$$

where Ω_{BZ} is the volume of the Brillouin zone. The distribution of $\lambda_{n\boldsymbol{k}}$ is shown in Fig. 4(a). It displays a significant anisotropy with a distribution in the 0.95–2.25 range. Then momentum $\boldsymbol{k}$-resolved EP coupling parameter $\lambda_{\boldsymbol{k}} = \sum_n \lambda_{n\boldsymbol{k}}$, with the sum over the electron states within ±200 meV from the Fermi energy. The variation of $\lambda_{\boldsymbol{k}}$ on the Fermi surface is shown in Fig. 4(b). It displays a significant anisotropy. The behavior of its complex variation is probably due to its complex Fermi surface shown in Fig. 2(b). We see that $\lambda_{\boldsymbol{k}}$ is especially high near the $\bar{K}$ point, where the largest spin-splitting occurs.

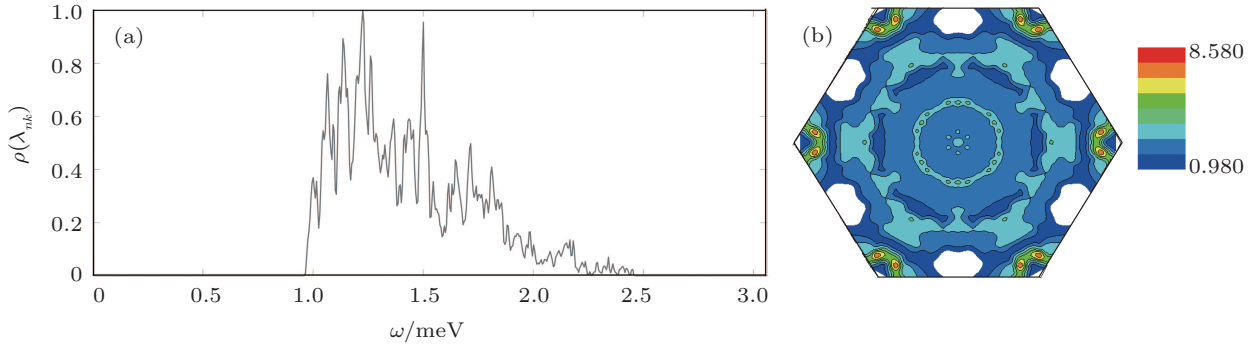


Fig. 4. (color online) (a) The distribution of $\lambda_{n\boldsymbol{k}}$ for Pb/$MoTe_2$/Pb heterostructure. (b) The variation of $\lambda_{n\boldsymbol{k}}$ on the Fermi surface, the data points correspond to electrons within ±200 meV from the Fermi energy.

The superconducting properties of the Pb/$MoTe_2$/Pb heterostructure are obtained by solving the following anisotropic Migdal–Eliashberg equations[43–46]

$$Z_{n\boldsymbol{k}}(i\omega_j) = 1 + \frac{\pi T}{N_{\mathrm{F}}\omega_j} \sum_{mj'} \int \frac{\mathrm{d}\boldsymbol{q}}{\Omega_{\mathrm{BZ}}} \frac{\omega_{j'}}{\sqrt{\omega_{j'}^2 + \triangle_{m\boldsymbol{k}+\boldsymbol{q}}^2(\mathrm{i}\omega_{j'})}} \times \delta(\varepsilon_{m\boldsymbol{k}+\boldsymbol{q}} - \varepsilon_{\mathrm{F}}) \lambda_{n\boldsymbol{k},m\boldsymbol{k}+\boldsymbol{q}}(\omega_j - \omega_{j'}), \tag{4}$$

$$Z_{n\boldsymbol{k}}(\mathrm{i}\omega_j)\Delta_{n\boldsymbol{k}}(\mathrm{i}\omega_j) = \frac{\pi T}{N_{\mathrm{F}}} \sum_{mj'} \int \frac{\mathrm{d}\boldsymbol{q}}{\Omega_{\mathrm{BZ}}} \frac{\triangle_{m\boldsymbol{k}+\boldsymbol{q}}(\mathrm{i}\omega_{j'})}{\sqrt{\omega_{j'}^2 + \triangle_{m\boldsymbol{k}+\boldsymbol{q}}^2(\mathrm{i}\omega_{j'})}} \times \delta(\varepsilon_{m\boldsymbol{k}+q} - \varepsilon_{\mathrm{F}}) [\lambda_{n\boldsymbol{k},m\boldsymbol{k}+\boldsymbol{q}}(\omega_j - \omega_{j'}) - \mu^*], \tag{5}$$

where $Z_{n\boldsymbol{k}}(\mathrm{i}\omega_j)$ is the mass renormalization function, $\omega_j = (2j+1)\pi T$ (with j being an integer and T the absolute temperature) are Fermion Matsubara frequencies, $\Delta_{n\boldsymbol{k}}(\mathrm{i}\omega_j)$ is the superconducting gap function, $\lambda_{n\boldsymbol{k},m\boldsymbol{k}+\boldsymbol{q}}(\omega_j - \omega_{j'})$ is the momentum- and energy-dependent EP interaction, and μ^* is the semiempirical Coulomb parameter. The anisotropic $\lambda_{n\boldsymbol{k},m\boldsymbol{k}+\boldsymbol{q}}(\omega_j - \omega_{j'})$ to be used in the Eliashberg equations is given by

$$\lambda_{n\boldsymbol{k},m\boldsymbol{k}+\boldsymbol{q}}(\omega_j) = N_{\mathrm{F}} \sum_{\nu} \int_0^{\infty} \mathrm{d}\omega \frac{2\omega}{\omega_j^2 + \omega^2} |g_{mn\nu}(\boldsymbol{k},\boldsymbol{q})|^2 \times \delta(\omega - \omega_{\boldsymbol{q}\nu}). \tag{6}$$

The equations are first solved self-consistently along the imaginary axis and then the gap at real-valued frequencies is obtained via Padé approximants.[47,48]

The superconducting gap $\Delta_{\boldsymbol{k}}$ on different parts of the Fermi surface at 1 K is shown in Fig. 5(a). We find that the distribution feature is very similar to that for EP coupling parameter $\lambda_{\boldsymbol{k}}$ shown in Fig. 4(b). It also displays a significant anisotropy. Figure 5(b) shows the superconducting energy gap $\Delta_{\boldsymbol{k}}$ as a function of temperature, calculated for a screened Coulomb parameter $\mu^* = 0.1$. The average value of the gap at each temperature is shown by square and Δ_0 is about 1.10 meV in the $T = 0$ K limit. The superconducting T_{c} is identified as the highest temperature at which the gap vanishes. From Fig. 5(b) we obtain $T_{\mathrm{c}} = 6.5$ K. This value is larger than the value ($T_{\mathrm{c}} = 5.6$ K) when Allen–Dynes equation is used to estimate the superconducting transition temperature. Our obtained ratio $\alpha = \Delta_0/k_{\mathrm{B}}T_{\mathrm{c}} = 1.955$, which is larger than the ideal BCS value of 1.764.[49] The BCS gap equation is given by [50]

$$\int_0^{k_{\mathrm{B}}\Theta_{\mathrm{D}}} \frac{\mathrm{d}\varepsilon}{E} \tanh\left(\frac{E}{2k_{\mathrm{B}}T}\right) = \ln\left(\frac{2\Theta_{\mathrm{D}}}{\alpha T_{\mathrm{c}}}\right), \tag{7}$$

Where $E = \sqrt{\varepsilon^2 + \Delta^2}$ and Θ_{D} is Debye temperature. By solving the BCS gap equation numerically, the temperature dependence of the superconducting gap is fitted and is shown in Fig. 5(b). The blue dashed line is obtained when α is taken as our calculated value (1.955). The green solid line is obtained when α is taken as the ideal BCS value (1.764).[49] It can fit our data at the temperature approaching T_{c}. Different α is needed in the BCS gap equation, probably because of strong anisotropy of the EP interaction. For completeness, we also explore the sensitivity of the calculated superconducting energy gap and critical temperature to the choice of the Coulomb parameter μ^*, as shown in Figs. 5(c) and 5(d). For $\mu^* = 0$, 0.05, and 0.12, we obtain $\Delta_0 = 1.83$, 1.32 and 1.02 meV and $T_{\mathrm{c}} = 10.0$, 7.8 and 6.3 K, respectively.

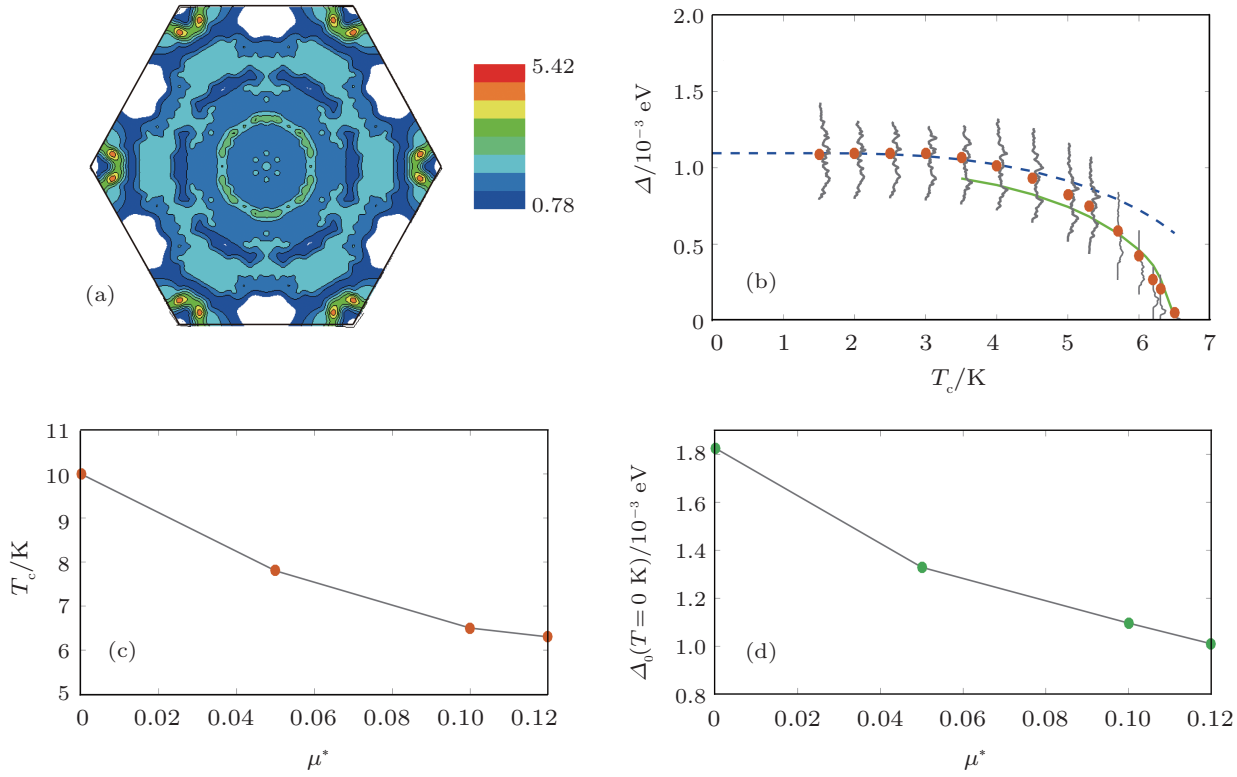


Fig. 5. (color online) (a) The superconducting gap at 1 K within ±200 meV from the Fermi energy, (b) energy distribution of the anisotropic superconducting gap Δ_k of Pb/$MoTe_2$/Pb heterostructure as a function of temperature, (c) calculated superconducting critical temperature as a function of the Coulomb parameter μ^*, and (d) calculated superconducting gap at the Fermi level in the $T = 0$ K limit as a function of the Coulomb parameter μ^*.

The Pb/$MoTe_2$/Pb heterostructure is a low-dimensional system with A complex Fermi surface, so the isotropic Migdal–Eliashberg equation is inadequate. Our calculated results show that the EP interaction has significant anisotropy. The temperature dependence of the superconducting gap can be fitted by solving the BCS gap equation numerically, but with an adjustable parameter α. These results provide support for a conventional phonon-mediated mechanism as the superconducting origin. Furthermore, in the Pb/$MoTe_2$/Pb heterostructure, the spin-splitting is completely out-of-plane and opposite at the $\bar{K}$ and $\bar{K}'$ points, and we find that the value of the spin-splitting near $\bar{K}$ point is much larger than the superconducting gap. This case is very similar to the case in monolayer transition metal dichalcogenides, the pairing state can be interpocket pairing (spin-singlet) or intrapocket pairing (spin-triplet) as suggested by Hsu *et al.*,[51] which suggests that the Pb/$MoTe_2$/Pb heterostructure may be a candidate for topological superconductors. Artificially engineered topological superconductivity in hybrid structures is currently attracting significant attention. Experimentally, proximity-induced superconductivity at the edges of nanowires has been studied by many groups and there is accumulating evidence in the search for Majorana fermions.[52,53] Regarding the semiconductors with Rashba-split bands, there has been no experiment so far on a 2D system according to the best of the author's knowledge. The Pb/$MoTe_2$/Pb heterostructure may be of interest for further experimental study.

4. Conclusions

In summary, we have investigated the peculiar electronic structures of the Pb/$MoTe_2$/Pb heterostructure by using density-functional theory. Due to strong SOC and space inversion asymmetry, large Rashba spin-splitting of electronic bands appears in this hybrid system. We have also studied superconducting properties of the Pb/$MoTe_2$/Pb heterostructure within the anisotropic Migdal–Eliashberg theory. Due to the complex Fermi surface in this low-dimensional system, the EP interaction and the superconducting gap display significant anisotropy. The temperature dependence of the superconducting gap can be fitted by solving the BCS gap equation numerically, but with an adjustable parameter α, suggesting a phonon-mediated mechanism as its superconducting origin. The spin-splitting near the $\bar{K}$ point is much larger than the superconducting gap, implying that the Pb/$MoTe_2$/Pb heterostructure may be a candidate for topological superconductivity.

References

[1] Hu G, Huang J Q, Wang Y N, Yang T, Dong B J, Wang J Z, Zhao B, Ali S and Zhang Z D 2018 *Chin. Phys. B* **27** 086301
[2] Tang F D, Wang P P, Wang P, Gan Y, Wang L, Zhang W and Zhang L Y 2018 *Chin. Phys. B* **27** 087307
[3] Geim A K and Novoselov K S 2007 *Nat. Mater.* **6** 183
[4] Zeng F, Zhang W B and Tang B Y 2015 *Chin. Phys. B* **24** 097103
[5] Radisavljevic B, Radenovic A, Brivio J, Giacometti V and Kis A 2011 *Nat. Nanotechnol.* **6** 147
[6] Wang Y Y, Quhe R G, Yu D P and Lü J 2015 *Chin. Phys. B* **24** 087201
[7] Benameur M M, Radisavljevic B, Heron J S, Sahoo S, Berger H and Kis A 2011 *Nanotechnology* **22** 125706
[8] Coleman J N, Lotya M, O'Neill A, *et al.* 2011 *Science* **331** 568
[9] Lee C, Li Q Y, Kalb W, Liu X Z, Berger H and Carpick R W 2010 *J. Hone, Science* **328** 76
[10] Splendiani A, Sun L, Zhang Y, Li T, Kim J, Chim C Y, Galli G and Wang F 2010 *Nano Lett.* **10** 1271
[11] Mak K F, Lee C, Hone J, Shan J and Heinz T F 2010 *Phys. Rev. Lett.* **105** 136805
[12] Li T and Galli G 2007 *J. Phys. Chem. C* **111** 16192
[13] Klein A, Tiefenbacher S, Eyert V, Pettenkofer C and Jaegermann W 2001 *Phys. Rev. B* **64** 205416
[14] Albe K and Klein A 2002 *Phys. Rev. B* **66** 073413
[15] Ding Y, Wang Y, Ni J, Shi L, Shi S and Tang W 2011 *Physica B* **406** 2254
[16] Kuc A, Zibouche N and Heine T 2011 *Phys. Rev. B* **83** 245213
[17] Mak K F, He K L, Shan J and Heinz T F 2012 *Nat. Nanotechnol.* **7** 494
[18] Xiao D, Liu G B, Feng W X, Xu X D and Yao W 2012 *Phys. Rev. Lett.* **108** 196802
[19] Ruppert C, Aslan O B and Heinz T F 2014 *Nano. Lett.* **146** 6231
[20] Qi J S, Li X, Niu Q and Feng J 2015 *Phys. Rev. B* **92** 121403
[21] Zhang Q Y, Yang S Y A, Mi W B, Cheng Y C and Schwingenschlögl U 2015 *Adv. Mater.* **28** 959
[22] Liu X, Du X and Huang G Q 2016 *Solid State Commun.* **248** 43
[23] Kallatt S, Umesh G, Bhat N and Maiumdar K 2016 *Nanoscale* **8** 15213
[24] Chen Q, Ouyang Y X, Yuan S J, Li R and Wang I L 2014 *ACS Appl. Mater. Interfaces* **6** 16835
[25] Lee K, Yun W S and Lee J D 2015 *Phys. Rev. B* **91** 125420
[26] Huang G Q, Xing Z W and Xing D Y 2016 *Phys. Rev. B* **93** 104511
[27] Wang Z Y, Xia W and Huang G Q 2017 *Physica C* **543** 52
[28] Pan S, Liu Q M, Ming F F, Wang K and Xiao X D 2011 *J. Phys.: Condens. Matter* **23** 485001
[29] Du X, Wang Z Y and Huang G Q 2016 *Mater. Res. Express* **3** 116302
[30] Li K, Feng X, Zhang W H, *et al.* 2013 *Appl. Phys. Lett.* **103** 062601
[31] Xue M Q, Chen G F, Yang H X, Zhu Y H, Wang D M, He J B and Cao T B 2012 *J. Am. Chem. Soc.* **134** 6536
[32] Zhang J J, Gao B and Dong S 2016 *Phys. Rev. B* **93** 155430
[33] Huang G Q, Xing Z W and Xing D Y 2015 *Appl. Phys. Lett.* **106** 113107
[34] Hamann D R 2013 *Phys. Rev. B* **88** 085117
[35] Giannozzi P et al. 2009 *J. Phys.: Condens. Matter* **21** 395502
[36] Perdew J P, Burke K and Ernzerhof M 1996 *Phys. Rev. Lett.* **77** 3685
[37] Mostofi A A, Yates J R, Lee Y S, Souza I, Vanderbilt Dand Marzari N 2008 *Comput. Phys. Commun.* **178** 685
[38] Ponce S, Margine E R, Verdi C and Giustino F 2016 *Comput. Phys. Commun.* **209** 116
[39] Jiang T, Liu H R, Huang D, Zhang S, Li Y G, Gong X G, Shen Y R, Liu W T and Wu S W 2014 *Nat. Nanotechnol.* **9** 825
[40] Wilson J A and Yoffe A D 1969 *Adv. Phys.* **18** 193
[41] Grimvall G 1981 *The Electron–Phonon Interaction in Metals* (New York: North-Holland)
[42] Allen P B 1983 *Solid State Phys.* **37** 1
[43] Allen P B and Mitrović B 1982 *Solid State Phys.* **37** 1
[44] Margine E R anf Giustino F 2013 *Phys. Rev. B* **87** 024505
[45] Choi H J, Roundy D, Sun H, Cohen M L and Louie S G 2002 *Nature* **418** 758
[46] Choi H J, Roundy D, Sun H, Cohen M L and Louie S G 2002 *Phys. Rev. B* **66** 020513
[47] Vidberg H J and Serene J W 1977 *J. Low Temp. Phys.* **29** 179
[48] Leavens C R and Ritchie D S 1985 *Solid Stata Commun.* **53** 137
[49] Bardeen J, Cooper L N and Schrieffer J R 1957 *Phys. Rev.* **108** 1175
[50] Johnston D C 2013 *Supercond. Sci. Technol.* **26** 115011
[51] Hsu Y T, Vaezi A, Fischer M H and Kim E A 2017 *Nat. Commun.* **8** 14985
[52] Mourik V, Zuo K, Frolov S M, *et al.* 2012 *Science* **336** 1003
[53] Das A, Ronen Y, Most Y, *et al.* 2012 *Nat. Phys.* **8** 887